INSTITUTE OF PHYSICS PUBLISHING JOURNAL OF PHYSICS B: ATOMIC, MOLECULAR AND OPTICAL PHYSICS

J. Phys. B: At. Mol. Opt. Phys. **37** (2004) 2411–2428 PII: S0953-4075(04)77202-8

The role of target polarization in electron–ion recombination

A V Korol[1], F J Currell[2] and G F Gribakin[3]

[1] Department of Physics, St Petersburg State Maritime Technical University, Leninskii prospect 101, St Petersburg 198262, Russia
[2] Department of Physics, Queen's University of Belfast, Belfast BT7 1NN, UK
[3] Department of Applied Mathematics and Theoretical Physics, Queen's University of Belfast, Belfast BT7 1NN, UK

E-mail: korol@rpro.ioffe.rssi.ru, f.j.currell@qub.ac.uk and g.gribakin@am.qub.ac.uk

Received 5 March 2004
Published 20 May 2004
Online at stacks.iop.org/JPhysB/37/2411
DOI: 10.1088/0953-4075/37/11/017

Abstract

We investigate the role of dynamic polarization of the target electrons in the process of recombination of electrons with multicharged ions (polarizational recombination). Numerical calculations carried out for a number of Ni- and Ne-like ions demonstrate that the inclusion of polarizational recombination leads to a noticeable increase (up to 30%) in the cross sections for incident electron energies outside the regions of dielectronic resonances. We also present a critical analysis of theoretical approaches used by other authors to describe the phenomenon of polarizational recombination.

(Some figures in this article are in colour only in the electronic version)

1. Introduction

In this paper we present analytical and numerical results of our study of the role of the so-called 'polarizational mechanism' in the process of recombination of electrons with multiply charged ions. Polarizational recombination is a mechanism in which the recombination photon is emitted by the target electrons, disturbed (polarized) by the incident electron. We demonstrate that for moderate non-relativistic energies of the incoming electron, $\varepsilon_1 = 0.5$–10 keV, the effect of polarizational recombination noticeably enhances the recombination cross sections for photon energies outside the regions dominated by dielectronic recombination. The magnitude of the effect is 10–30% for Ne-like and Ni-like ions.

The most important energy loss mechanisms from high temperature plasmas such as those found in solar and laboratory fusion environments are driven by interactions between multiply charged ions and electrons. Radiation losses originating from dielectronic recombination and radiative recombination are dominant and can have a marked effect on the plasma charge

 © 2004 IOP Publishing Ltd Printed in the UK

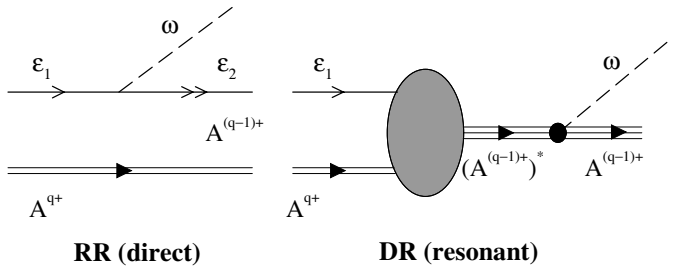

Figure 1. Schematic representation of the RR and DR processes. In the RR diagram ε_1 and ε_2 denote the initial and final states of the incident electron in the field of the target ion A^{q+}, and the dashed line shows the emitted photon. In the DR diagram the shaded area describes the electron interaction(s) leading to the capture of the incident electron in the quasi-bound state $(A^{(q-1)+})^*$, which is then stabilized radiatively.

balance and electron temperature. Hence, it is important to evaluate rates for these processes. This in turn leads to the requirement of reliable total recombination cross sections as a function of energy. In particular, polarizational recombination must be correctly included for many-electron multiply charged ions such as those discussed in this paper if reliable cross sections and rates are to be obtained.

Furthermore, in experimental investigations, other cross sections are commonly normalized to radiative recombination cross sections. For example, all experimentally determined hydrogen-like highly charged ion cross sections available for a nuclear charge greater than 20 have been normalized in this way (Watanabe *et al* 2002) as have dielectronic recombination cross sections (see, e.g., Smith *et al* (2000), or O'Rourke *et al* (2004)). If these types of experimental studies are to be extended to many-electron multiply charged ions, then reliable non-resonant recombination cross sections seem requisite. Recent experiments using heavy-ion accelerators and storage rings have provided increased amounts of information on absolute values of the recombination cross sections at high energy resolution (see Kilgus *et al* (1992), Schenach *et al* (1994), DeWitt *et al* (1994), and more recent work from these groups, e.g., Hoffknecht *et al* (1998), Schnell *et al* (2003), Schuch *et al* (2003)). This allows one to make direct comparisons between experimental and theoretical cross sections (see, e.g., Schippers *et al* (2002) and Tokman *et al* (2002)).

Theoretically, the process of recombination in binary electron–ion collisions is usually considered in terms of two main mechanisms: radiative recombination (RR) and dielectronic recombination (DR) (see, e.g., Hahn (1997)).

RR is a direct process $e^- + A^{q+} \rightarrow A^{(q-1)+} + \omega$ in which an electron, initially in a continuous spectrum state, undergoes a free-bound transition in the static field of the target ion A^{q+} (q stands for the ionicity), accompanied by the emission of a photon which carries away the excess energy ω. In the final state, $A^{(q-1)+}$, the electron is bound to the target.

DR stands for the two-step process: $e^- + A^{q+} \rightarrow (A^{(q-1)+})^* \rightarrow A^{(q-1)+} + \omega$. Here, in the first stage, the incoming electron and the target ion form a quasi-bound excited state of the compound ion, $(A^{(q-1)+})^*$. This capture is only possible if ε_1 is close to the difference between the total energy of $(A^{(q-1)+})^*$ and that of A^{q+}. The second stage of the process is a radiative decay of the excited compound ion state. Both processes are illustrated in figure 1.

The main difference between RR and DR is that the latter is a resonant process. Its contribution manifests itself as a set of peaks over the smooth RR background. The positions and the widths of these peaks are related to the energies and widths of the allowed intermediate excited states $(A^{(q-1)+})^*$.

Another difference is that the final state of RR is assumed to be that of an electron moving in the field of the (ground-state) target ion. In contrast, the final states populated in DR include doubly excited states of the compound ion. Of course, the final states formed in RR can also result from the DR process. However, their contribution to the DR cross section is by no means dominant, since most DR resonances have many radiative decay channels. As a result, one can often neglect the interference between RR and DR and obtain the total recombination cross section as a sum of the smooth RR background and DR peaks.

The quantitative characteristics of the recombination process include, in particular, the cross section of *selective* recombination, $\sigma(\nu_2)$, when the electron is captured into the final state, ν_2, (characterized, e.g., by the principal quantum number n_2 and orbital angular momentum l_2, if one adopts a non-relativistic description), and the total cross section, $\sigma = \sum_{\nu_2} \sigma(\nu_2)$, when the final state is not specified.

As a function of ε_1, the recombination cross section varies rapidly in those regions where DR resonances occur. DR often dominates over RR, leading to $\sigma(\nu_2) \approx \sigma_{\mathrm{DR}}(\nu_2)$. For electron energies outside such regions $\sigma(\nu_2) \approx \sigma_{\mathrm{RR}}(\nu_2)$, and the cross section exhibits smooth behaviour. For electron capture accompanied by the target excitation from the jth subshell, the range of incident electron energies ε_1 where DR resonances occur is given by

$$I_j - 2I_e < \varepsilon_1 < I_j, \tag{1}$$

where I_j is the ionization potential of subshell j, and I_e is the ionization energy of the lowest unoccupied (excited state) orbital. In multicharged many-electron ions the ionization potentials of different subshells are well separated. Therefore, there exist wide ranges of incident electron energies where the cross section is free from the DR resonances.

It is the aim of our paper to demonstrate that for electron energies *outside* the DR resonance regions, defined by (1), the recombination cross section $\sigma(\nu_2)$ is enhanced compared to $\sigma_{\mathrm{RR}}(\nu_2)$. This increase is due to the contribution of another distinct mechanism of recombination, the polarizational recombination (PR) (Connerade and Solov'yov 1996, Bureeva and Lisitsa 1998). The PR mechanism is somewhat similar to 'radiative dielectronic recombination' (Hahn 1997), characterized by off-shell excitations of the target electrons. It was considered by Hahn (1997) and deemed 'difficult to estimate'. It is closely related to the polarizational bremsstrahlung (Amusia 1982, 1988, Korol and Solov'yov 1997). In the latter, the photon emission occurs due to *virtual* excitations (polarization) of the target electrons by the Coulomb field of the projectile. The polarizational mechanism plays an important role in forming the bremsstrahlung spectrum of electrons over wide ranges of photon energies (see, e.g., Korol *et al* (1997)). The bremsstrahlung and recombination processes are similar, differing only in the type of radiative transition involved: the former corresponds to a free–free transition, whereas the latter requires a free-bound one.

The PR mechanism was earlier studied by Connerade and Solov'yov (1996) in application to collisions of electrons with clusters. They demonstrated that the polarizational mechanism gives rise to a giant resonance in the recombination cross section. In the vicinity of the resonance, which is related to the giant resonance in the photoionization of the cluster, the recombination cross section is dominated by PR.

For electron collisions with multicharged ions, the PR mechanism was considered by Bureeva and Lisitsa (1998, 1999) and further discussed by Astapenko *et al* (2000, 2002). Using the arguments of classical mechanics, they derived a simple approximate formula for the contribution of PR and for the ratio of the PR and RR cross sections[4]:

$$\frac{\sigma_{\mathrm{PR}}(\nu_2)}{\sigma_{\mathrm{RR}}(\nu_2)} \approx \left| \frac{\omega^2 \alpha(\omega)}{Z_{\mathrm{eff}}} \right|^2, \tag{2}$$

[4] Atomic units are used throughout the paper.

where $\alpha(\omega)$ is the dynamic dipole polarizability of the target, and $Z_{\rm eff}$ is the charge seen by the projectile at some effective distance, r_0, from the nucleus (see Bureeva and Lisitsa 1998, Kogan *et al* 1992). The radius r_0 depends on ε_1 and ω. It is found as the root of the equation (Bureeva and Lisitsa 1998)

$$\varepsilon_1 = -\frac{Z}{r_0} + U_{\rm el}(r_0) + \frac{\omega^2 r_0^2}{2}, \tag{3}$$

where Z is the nuclear charge and $U_{\rm el}(r)$ is the electrostatic potential of the target electrons. By definition, $Z_{\rm eff} = Z - r_0 U_{\rm el}(r_0)$. For low electron energies $Z_{\rm eff}$ reduces to the net ionic charge, Z_0, while for large ε_1 and ω it becomes equal to Z. Based on their estimate (2), Bureeva and Lisitsa (1998) claimed that 'the contribution of PR to the total recombination rates may be comparable to or exceed (by more than an order of magnitude) the standard contribution of radiative recombination'.

However, estimate (2) should be used with caution. In a recent calculation (Gribakin and Korol 2001) we found that this relation could greatly overestimate the contribution of the PR mechanism to the cross section. In particular, we examined the contribution of PR to the recombination of electrons with Au^{25+} within the energy range $\varepsilon_1 = 0.01$–100 eV. It was found that for the dominant channels of recombination into the low-lying states, equation (2) overestimated the contribution of PR by up to two orders of magnitude, in comparison with the results of more accurate calculations. For the capture into high Rydberg states, equation (2) did reproduce the ratio of the cross sections correctly, but in that case the contribution of the PR mechanism was negligibly small compared to RR.

In what follows we present the results of calculations of the contribution of PR mechanism in electron collisions with a number of Ni- and Ne-like ions. In particular, we demonstrate that PR leads to an increase of the cross section, mostly due to the interference between the RR and PR amplitudes. This enhancement is much smaller than predicted by Bureeva and Lisitsa (1998, 1999) and Astapenko *et al* (2000, 2002). On the other hand, the contribution of PR seems to be more significant than estimated by Hahn (1997).

2. Formalism

To describe the RR and PR contributions, let us consider the incoming electron moving in the static spherically symmetric potential of an ion in the ground state. The electron wavefunction in the non-relativistic distorted partial wave approximation is given by (see, e.g., Landau and Lifshitz (1977))

$$\Psi^{(+)}_{\mathbf{p}_1}(\mathbf{r}) = \frac{4\pi}{p_1} \sum_{l_1 m_1} \mathrm{i}^{l_1}\, \mathrm{e}^{\mathrm{i}\delta_{l_1}(p_1)} Y^*_{l_1 m_1}(\mathbf{p}_1/p_1) Y_{l_1 m_1}(\mathbf{r}/r) r^{-1} P_{\nu_1}(r), \tag{4}$$

where $\mathbf{p}_1$ is the electron momentum, $Y_{l_1 m_1}$ are the spherical harmonics, $P_{\nu_1}(r)$ is the radial Hartree–Fock wavefunction in the frozen-core ionic potential, ν_1 stands for the energy $\varepsilon_1 = p_1^2/2$ and orbital angular momentum l_1 of the electron, and $\delta_{l_1}(p_1)$ is the scattering phase shift which includes the Coulomb correction due to the net ionic charge Z_0.

The amplitude of RR is a single-electron bound-free dipole matrix element,

$$F_{\rm RR} = \langle 2|\mathbf{e}\cdot\mathbf{r}|1\rangle \equiv \int \mathrm{d}\mathbf{r}\, \Psi^*_{n_2 l_2 m_2}(\mathbf{r})\, \mathbf{e}\cdot\mathbf{r}\, \Psi^{(+)}_{\mathbf{p}_1}(\mathbf{r}), \tag{5}$$

where $\mathbf{e}$ is the vector of the photon polarization, and $\Psi_{n_2 l_2 m_2}(\mathbf{r}) = Y_{l_2 m_2}(\hat{\mathbf{r}}) P_{\nu_2}(r)/r$ is the final bound-state wavefunction of the captured electron with energy $\varepsilon_2 < 0$. The energy of the emitted photon is given by $\omega = \varepsilon_1 - \varepsilon_2$.

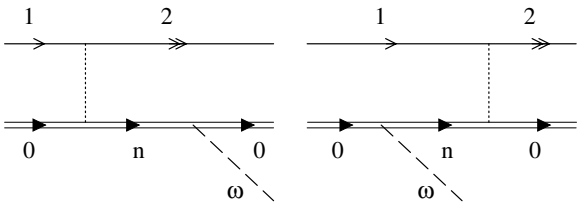

Figure 2. Diagrammatic representation of the PR amplitude. The upper solid line describes the transition of the incident electron from the initial state '1' into the final bound state '2'. The double line corresponds to the target ion A^{q+}: '0' denotes its initial and final states, and 'n' refers to the intermediate, virtual, state. Vertical dashed lines indicate the Coulomb interaction between the projectile and the ion, and long-dashed lines describe the emitted photon.

In the same approximation, the PR amplitude is described by a compound matrix element. It accounts for non-radiative capture of the projectile due to the Coulomb interaction with the target electrons, accompanied by the formation of a virtual excited state of the target, which decays via the emission of a photon. One should also allow for the alternate time sequence of the two events. The corresponding diagrams are shown in figure 2.

Analytically, the PR amplitude is given by the following expression:

$$F_{\mathrm{PR}} = -\sum_{a,a'=1}^{N}\sum_{n}\left[\frac{\langle 0|\mathbf{e}\cdot\mathbf{r}_a|n\rangle\langle n;\,2|v_{a'}|1;\,0\rangle}{\omega_{n0}-\omega}+\frac{\langle 0;\,2|v_{a'}|1;\,n\rangle\langle n|\mathbf{e}\cdot\mathbf{r}_a|0\rangle}{\omega_{n0}+\omega}\right], \tag{6}$$

where a and a' enumerate the target electrons of the total number N, $\mathbf{r}_a$ is the radius-vector of the ath electron and $v_a = 1/|\mathbf{r}-\mathbf{r}_a|$ is its Coulomb interaction with the incident electron. The sum $\sum_n$ is carried out over the whole spectrum of excited states of the target, including excitations into the continuum. Effectively, only the states allowed by the dipole selection rules contribute to the sum. The quantity $\omega_{n0} = \varepsilon_n - \varepsilon_0$ is the transition energy.

When the photon energy ω is close to the excitation energy ω_{n0} of a discrete spectrum state n ($\varepsilon_n < 0$), the PR amplitude is resonantly enhanced. This enhancement corresponds to a dielectronic resonance at $\varepsilon_1 \approx \varepsilon_2 + \varepsilon_n - \varepsilon_0$, where amplitude (6) is dominated by the single term

$$F_{\mathrm{PR}}|_{\omega\approx\varepsilon_n-\varepsilon_0} \approx -\frac{\langle 0|\mathbf{e}\cdot\mathbf{D}|n\rangle\langle n;\,2|V|1;\,0\rangle}{\varepsilon_n-\varepsilon_0-\omega-\mathrm{i}\Gamma_n/2}, \tag{7}$$

where $\mathbf{D} = \sum_{a=1}^{N}\mathbf{r}_a$ and $V = \sum_{a=1}^{N} v_a$. We have also introduced the total width Γ_n of the intermediate state in the denominator, to describe accurately the behaviour of the amplitude near the pole. The amplitude $\langle 0|\mathbf{e}\cdot\mathbf{D}|n\rangle$ determines the partial radiative width of the state n due to the transition $n \to 0$, $\Gamma_{n0}^{(\gamma)} \propto |\langle 0|\mathbf{e}\cdot\mathbf{D}|n\rangle|^2$.

The structure of the right-hand side of (7) shows that the resonant part of the PR amplitude accounts for the DR processes leading to the final state with a single excited electron. Therefore, in the region of dielectronic resonances the PR mechanism is indistinguishable from the DR mechanism.

In this paper, we are interested in the role of the PR mechanism within the energy intervals which are free from DR resonances (both of the type discussed above and more complex ones, which are included in the full treatment of DR). For such energies the total amplitude of the recombination process is given by the sum of F_{RR} and the (non-resonant) PR amplitude (6):

$$F_{\mathrm{tot}} = F_{\mathrm{RR}} + F_{\mathrm{PR}}. \tag{8}$$

The cross section is proportional to the modulus squared of the amplitude $F_{\rm tot}$. Hence, it can be written as a sum of three terms,

$$\sigma_{\rm tot} = \sigma_{\rm RR} + \sigma_{\rm int} + \sigma_{\rm PR}, \tag{9}$$

where $\sigma_{\rm RR} \propto |F_{\rm RR}|^2$ and $\sigma_{\rm PR} \propto |F_{\rm PR}|^2$ stand for the cross sections of the RR and PR processes, and $\sigma_{\rm int}$ is the interference term proportional to $\mathrm{Re}(F^*_{\rm RR}F_{\rm PR})$. Note that $\sigma_{\rm int}$ can be of either sign.

To calculate the contribution of PR, we assume that the ground and excited states of the target are described in the Hartree–Fock approximation. Such excited states correspond to electron–hole pairs. Applying the standard technique to obtain the cross section (see, e.g., Berestetsky *et al* (1982)) and carrying out the necessary angular momentum algebra (see, e.g., Varshalovich *et al* (1988)) one obtains the following expression for the cross section of selective radiative capture in the ν_2 state:

$$\sigma_{\rm tot}(\nu_2) = \frac{16\pi\omega^3}{3p_1^3c^3}\sum_{l_1=l_2\pm1} l_> \left(\mathcal{R}_{\nu_2\nu_1} + \mathcal{P}_{\nu_2\nu_1}\right)^2, \tag{10}$$

where $l_> = \max\{l_1, l_2\}$. The quantities $\mathcal{R}_{\nu_2\nu_1}$ and $\mathcal{P}_{\nu_2\nu_1}$ are the partial RR and PR amplitudes:

$$\mathcal{R}_{\nu_2\nu_1} \equiv r_{\nu_2\nu_1} = \int_0^\infty \mathrm{d}r\, P_{\nu_2}(r) r P_{\nu_1}(r), \tag{11a}$$

$$\mathcal{P}_{\nu_2\nu_1} = -\sum_{\nu_0}\frac{N_{\nu_0}}{2l_0+1}\sum_{\nu_n}\max\{l_0, l_n\}\frac{2\omega_{n0}r_{\nu_0\nu_n}V^{(1)}_{n2,10}}{\omega^2_{n0}-\omega^2}, \tag{11b}$$

where $V^{(1)}_{n2,10}$ denotes the radial matrix element of the dipole part of the Coulomb interaction:

$$V^{(1)}_{n2,10} = \frac{1}{3}\int_0^\infty\int_0^\infty \mathrm{d}r\,\mathrm{d}r' P_{\nu_n}(r') P_{\nu_2}(r)\frac{r_<}{r_>^2}P_{\nu_1}(r)P_{\nu_0}(r'), \tag{12}$$

and $r_>(r_<)$ is the largest (smallest) of r and r'.

The outer sum in (11*b*), $\sum_{\nu_0} \equiv \sum_{n_0l_0}$, is carried out over the orbitals n_0l_0 occupied in the ionic ground state, and N_{ν_0} stands for the number of electrons in the subshell ν_0. The inner sum, $\sum_{\nu_n} \equiv \sum_{\varepsilon_n l_n}$, is over the excited state orbitals (summation over ε_n also implies integration over the continuous spectrum of excitations).

In numerical calculations we use nonrelativistic Hartree–Fock wavefunctions and restrict ourselves to the case of low- and medium-Z targets. Electron correlations beyond the Hartree–Fock scheme have not been included. For multiply charged ions they are of minor importance.

To conclude this section we demonstrate, within our formalism, how one can derive expression (2) proposed by Bureeva and Lisitsa (1998). In doing so we will also establish the limits of validity of (2).

Equation (2) contains the dynamic dipole polarizability. This implies that effective distances between the projectile and the target, which are important for the PR mechanism, are greater than the average radius of the ion, R. This condition is well known in the theory of polarizational bremsstrahlung (see, e.g., Zon (1977), Amusia (1988) and Korol and Solov'yov (1997)), where it has a clear physical justification. The dipole polarization of the electron cloud is most pronounced if the Coulomb field of the projectile is uniform on the scale of R, i.e. when the projectile is outside the target, $r > R$. For small distances, $r \ll R$, this field is almost spherically symmetric. Therefore, it induces a small dipole moment on the target. Hence, small distances are less important. An extension of the 'large-distance approximation' to the process of polarizational capture should be done with care. In particular, it requires that

the wavelength of the projectile must be much greater than R (i.e. a low-ε_1 incoming electron) *and* the final state ν_2 must be a Rydberg state, whose effective radius also exceeds R.

Under these assumptions, the Coulomb interaction, which appears on the right-hand side of (6), can be expanded as $v_a \approx \mathbf{r}_a \cdot \mathbf{r}/r^3$, which allows one to express the PR amplitude in terms of the dynamic dipole polarizability $\alpha(\omega)$,

$$F_{\mathrm{PR}} \approx -\left\langle 2 \left| \frac{\mathbf{e}\cdot\mathbf{r}}{r^3} \right| 1 \right\rangle \alpha(\omega), \tag{13}$$

where

$$\alpha(\omega) = \frac{2}{3}\sum_n \frac{\omega_{n0}\,|\langle n|\mathbf{D}|0\rangle|^2}{\omega_{n0}^2 - \omega^2}. \tag{14}$$

The operator in (13) is proportional to $-Z_0\mathbf{r}/r^3$, which is the acceleration operator of the electron in the field $-Z_0/r$. The latter is equal to the electrostatic potential of the target in the region $r \gg R$. If one assumes that the initial- and final-state wavefunctions of the electron can be treated as solutions of the Schrödinger equation in the field of a point charge Z_0, then the matrix element of the acceleration in equation (13) can be converted into the matrix element of the operator $\mathbf{r}$ (see, e.g., Sobelman (1992)). This allows one to relate F_{PR} to the RR amplitude (5),

$$F_{\mathrm{PR}} \approx -\langle 2|\mathbf{e}\cdot\mathbf{r}|1\rangle \frac{\omega^2\alpha(\omega)}{Z_0} = -F_{\mathrm{RR}}\frac{\omega^2\alpha(\omega)}{Z_0}. \tag{15}$$

Consequently, the ratio of the cross sections is given by

$$\frac{\sigma_{\mathrm{PR}}(\nu_2)}{\sigma_{\mathrm{RR}}(\nu_2)} \approx \left| \frac{\omega^2\alpha(\omega)}{Z_0} \right|^2. \tag{16}$$

This formula coincides with (2) if one puts $Z_{\mathrm{eff}} = Z_0$ in the latter.

We would like to emphasize that the approximations tacitly made by Bureeva and Lisitsa (1998) in deriving their estimate (see section 2 of their paper) are equivalent to those made above. Hence, the distance r_0 defined by (3) and used in (2) must be greater than R. This means that in the range of validity of (2) one can put $Z_{\mathrm{eff}} = Z_0$, while for $r_0 < R$ (where $Z_{\mathrm{eff}} > Z_0$) the estimate (2) is not valid.

The condition $r_0 > R$ imposes restrictions on the range of values of ε_1 and ω for which one can rely on (16) when estimating the relative contribution of the PR channel. To establish these ranges, let us analyse equation (3) in the region $r_0 > R$. Replacing $Z/r_0 - U_{\mathrm{el}}(r_0)$ with Z_0/r, one obtains

$$\varepsilon_1 + \frac{Z_0}{r_0} = \frac{\omega^2 r_0^2}{2}. \tag{17}$$

From this equation it is clear that the radius r_0 is a decreasing function of ω. Therefore, for a given ε_1 the relation $r_0 = R$ defines $\omega_{\max}$, the maximum photon energy consistent with the large-distance approximation. Putting $r_0 = R$ one finds

$$\omega_{\max} = \frac{I}{n_*}\left(1 + \frac{\varepsilon_1}{I}\right)^{1/2}, \tag{18}$$

where I is the ionization potential of the target and n_* is the effective principal quantum number of the outermost occupied ionic orbital. In deriving (18) we used $I = Z_0^2/2n_*^2$ and evaluated R as the classical turning point of the outer-shell electron in the ionic field, $R \approx Z_0/I$.

Being the energy of the recombination photon, $\omega_{\max}$ must satisfy the conditions

$$\varepsilon_1 \leqslant \omega_{\max} < \varepsilon_1 + I. \tag{19}$$

Indeed, the extreme case $\omega_{\max} = \varepsilon_1$ corresponds to capture into the state with $\varepsilon_2 = 0$, whereas $\omega_{\max} \sim \varepsilon_1 + I$ results from capture into the lowest vacant orbital of the ion. For many-electron ions ($n_* \gg 1$) relations (18) and (19) lead to

$$\varepsilon_1 \ll I, \qquad \omega \ll I. \tag{20}$$

Hence, estimates (2) and (16) are only applicable to the capture of low-energy electrons into Rydberg states with principal quantum numbers $n_2 \gg n_*$.

However, for such ε_1 and n_2 the contribution of PR is small. Indeed, for $\omega \ll I$ the dynamic polarizability can be replaced by its static value $\alpha(0) \sim R^3/Z_0$. Then, using $R \approx Z_0/I$, one obtains from (16): $\omega^2\alpha(\omega)/Z_0 \sim (\omega/I)^2(R/a_0) \ll 1$ (a_0 is the Bohr radius). The same result can be obtained using other estimates of the static polarizability. For example, choosing $\alpha(0) \approx 4(Z - Z_0)^3/Z^4$ which corresponds to the Thomas–Fermi model (see [14] in Astapenko *et al* 2002), it is easy to demonstrate that $\omega^2\alpha(\omega)/Z_0 \leqslant (n_*/n_2)^4 \ll 1$.

It will be shown in the next section that outside the region of low ε_1 and large n_2 equations (2) and (16) grossly overestimate the role of PR.

3. Numerical results and discussion

The cross sections $\sigma_{\rm tot}, \sigma_{\rm RR}, \sigma_{\rm PR}$ and the interference terms have been calculated for a range of energies $\varepsilon_1 = 0.01$–5 keV of the electron incident on a number of Ni-like (isoelectronic sequence $1s^22s^22p^63s^23p^63d^{10}$) and Ne-like ($1s^22s^22p^6$) ions. The electronic structure of the final state is that of one electron in the nl orbital ($n \geqslant 4$ in the Ni-like case, and $n \geqslant 3$ for Ne-like ions) above the closed-shell target ground-state configuration.

In reporting our results, we use the following simplified notation: $\sigma(nl)$ is the cross section of selective capture into the nl state, $\sigma(n)$ denotes the sum $\sum_{l=0}^{n-1}\sigma(nl)$, and $\sigma(n_1 - n_2)$ stands for $\sum_{n=n_1}^{n_2}\sigma(n)$.

3.1. Ni-like ions

The calculations have been performed for Kr^{8+}, Zr^{12+}, Ru^{16+}, Sr^{20+}, Xe^{26+} and Ba^{28+}. Figure 3 shows the cross sections $\sigma_{\rm tot}(4)$, $\sigma_{\rm RR}(4)$ and $\sigma_{\rm PR}(4)$ as functions of ε_1 for Kr^{8+} and Xe^{26+}. As usual, the RR cross sections (dashed curves) exhibit a smooth monotonic behaviour, decreasing rapidly with the electron energy ε_1. The total (solid curves) and PR (dotted curves) cross sections display sharp maxima corresponding to discrete ionic excitations: in both figures the clump of peaks at low energies corresponds to resonant transitions from 3s, 3p and 3d orbitals, while that at higher energies is due to excitations from $n = 2$ shell. Outside the resonance regions $\sigma_{\rm tot}(4)$ and $\sigma_{\rm PR}(4)$ do not show any irregularities.

As explained in section 1, our prime interest is in determining the role of PR in the regions which are free of resonances. For Kr^{8+} and Xe^{26+} these are $\varepsilon_1 \approx 0.3$–1.5 keV and $\varepsilon_1 > 2$ keV in the case of Kr^{8+} and $\varepsilon_1 \approx 1.1$–3.9 keV for Xe^{26+}. Examining these regions in figure 3, one can clearly see the two main features of PR. First, the relative magnitude of $\sigma_{\rm PR}$ is very small, varying between 10^{-3} and 10^{-1} of $\sigma_{\rm RR}$. Accordingly, the ratio $\sigma_{\rm PR}/\sigma_{\rm RR}$ in non-resonant regions is much smaller than the values which can be inferred from (2). We will discuss this point in more detail later in this section.

The second feature is that the total cross section systematically exceeds the RR cross section in the non-resonant regions, although this effect is not large. Taking into account the relation $\sigma_{\rm PR}/\sigma_{\rm RR} \ll 1$ and recalling equation (9), one realizes that it is the interference term, $\sigma_{\rm int}$, which leads to this enhancement of the cross section. Hence, we can write

$$\frac{\sigma_{\rm tot}}{\sigma_{\rm RR}} \approx 1 + \frac{\sigma_{\rm int}}{\sigma_{\rm RR}}. \tag{21}$$

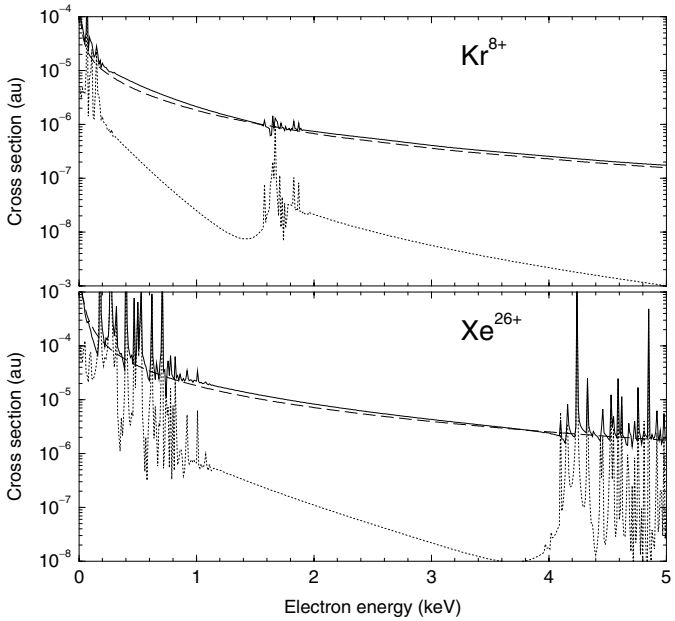

Figure 3. Radiative, polarizational and total recombination cross section for capture into the $n = 4$ states for Kr^{8+} (top) and Xe^{26+} (bottom): – – –, $\sigma_{RR}(4)$; · · · · · ·, $\sigma_{PR}(4)$; ——, $\sigma_{tot}(4)$.

For photon energies well above the ionization thresholds of many-electron subshells, the interference between the radiation emitted via RR and PR mechanisms is constructive and results in $\sigma_{int} > 0$ and, consequently, in $\sigma_{tot} > \sigma_{RR}$. A similar effect is also known in bremsstrahlung (e.g., Amusia 1988, Korol and Solov'yov 1997). It will be examined more closely further on in the paper.

These two features are typical for all Ni-like ions that we have investigated. They can also be seen in the cross sections of selective capture into the states with different orbital angular momenta, and into the states with $n_2 > 4$. Thus, in figure 4 we show the selective capture cross sections σ_{tot} and σ_{RR} for the 4s, 4p, 4d and 4f states in Kr^{8+} and Xe^{26+}. In the case of Xe^{26+} only the non-resonant interval of ε_1 is presented. For all channels the excess of σ_{tot} over σ_{RR} is clearly visible. Its origin is in the constructive interference between the photons emitted via the RR and PR mechanisms. The contributions of σ_{PR} (not shown in the figure) are negligibly small for all the channels.

A similar relationship between σ_{tot}, σ_{RR} and σ_{PR} in the non-resonant regions holds for the capture into the states with higher principal quantum numbers n_2, as illustrated by figure 5. Here, the coloured curves correspond to the cross sections $\sigma_{tot}(n_2)$ and $\sigma_{RR}(n_2)$ with $n_2 = 4$–7. Black curves represent the total and RR cross sections summed over n_2 from 4 up to 10. Again, the curves for σ_{PR} are not shown because of the strong inequality $\sigma_{PR} \ll \sigma_{tot}, \sigma_{RR}$.

The small sizes of σ_{PR} relative to σ_{RR} seem to be in contradiction with the estimates of Bureeva and Lisitsa (1998). To highlight the size of this discrepancy, in figures 6(a)–(d) we plot the ratio $\sigma_{PR}(4p)/\sigma_{RR}(4p)$ for Kr^{8+} and Xe^{26+} in the nonresonant regions, calculated using different approaches. Our numerical results in figures 6(a) and (b) show that the contribution of $\sigma_{PR}(4p)$ to the total cross section is at the level of ∼0.1–1%. To calculate the ratio $[\omega^2\alpha(\omega)/Z_{eff}]^2$, we take into account the relationship between the photon energy and that of the incoming electron: $\omega = \varepsilon_1 + I_{4p}$, where I_{4p} is for the Hartree–Fock ionization energy of

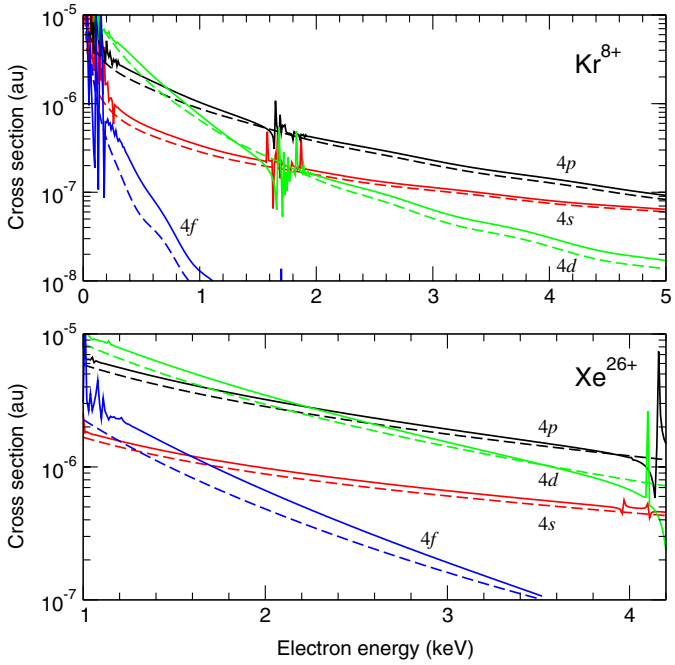

Figure 4. Recombination cross sections $\sigma_{\rm tot}(4l)$ (solid curves) and $\sigma_{\rm RR}(4l)$ (dashed curves) for capture into $l = 0, 1, 2, 3$ states, for Kr^{8+} (top) and Xe^{26+} (bottom). Red curves, 4s-states ($l = 0$); black curves, 4p-states ($l = 1$); green curves, 4d-states ($l = 2$); blue curves, 4f-states ($l = 3$).

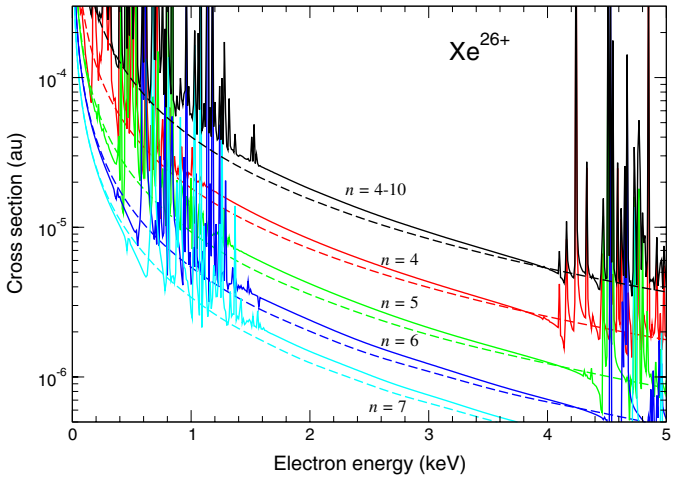

Figure 5. Total (solid curves) and RR (dashed curves) cross sections for the capture into orbitals with different principal quantum numbers in Xe^{26+}. Red curves correspond to $\sigma_{\rm tot}(n)$ and $\sigma_{\rm RR}(n)$ with $n = 4$; green curves, $n = 5$; blue curves, $n = 6$; cyan curves, $n = 7$. Black curves correspond to $\sigma_{\rm tot}$ (4–10) and $\sigma_{\rm RR}$ (4–10).

the 4p orbital (see table 1). The dynamical polarizability is evaluated in the Hartree–Fock approximation. The effective charge $Z_{\rm eff}$ for each pair of ε_1 and ω is found following the prescription of Bureeva and Lisitsa (1998), as $Z_{\rm eff} = Z - r_0 U_{\rm el}(r_0)$, where the radius r_0 is found by a numerical solution of equation (3). The electrostatic potential of the target

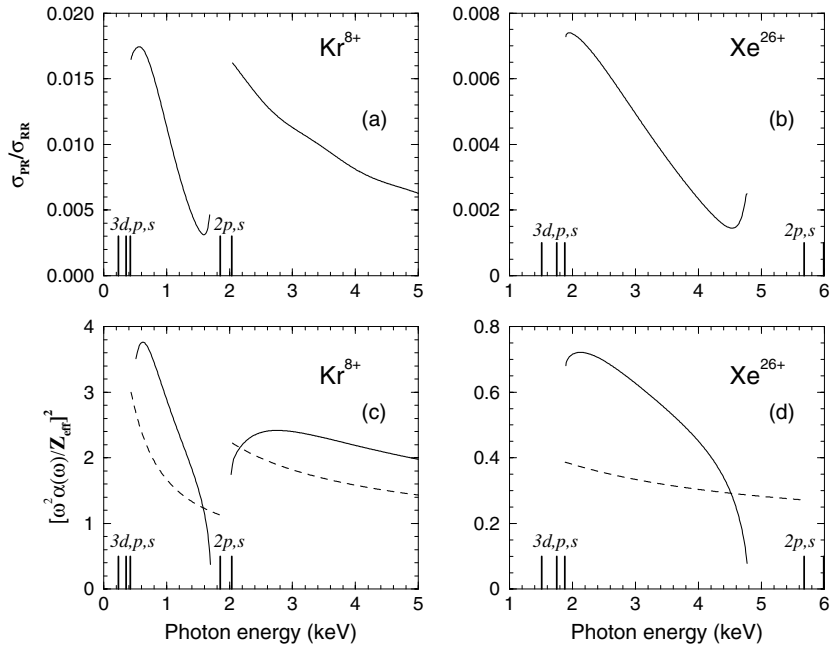

Figure 6. Ratios $\sigma_{PR}(4p)/\sigma_{RR}(4p)$ in non-resonant photon energy ranges for the selective capture to 4p states in Kr^{8+} and Xe^{26+}. (a) and (b) are the results of our numerical calculations. In (c) and (d) solid curves show estimate (2), and dashed curves show the results obtained from the approximate expression for $[\omega^2\alpha(\omega)/Z_{\rm eff}]^2$ (see explanations in the text). Vertical bars mark the ionization thresholds in the Hartree–Fock approximation (see table 1).

Table 1. Hatree–Fock ionization energies of the ground state orbitals and excited 4p orbital (in eV) for Ni-like ions.

Orbital	Kr^{8+}	Zr^{12+}	Ru^{16+}	Cd^{20+}	Xe^{26+}
1s	14 288	17 941	22 032	26 558	34 166
2s	2 037.3	2 721.1	3 516.4	4 422.2	5 986.7
2p	1 850.4	2 507.4	3 275.6	4 153.8	5 677.2
3s	427.3	662.7	948.2	1 283.0	1 876.9
3p	359.0	580.6	852.0	1 172.6	1 745.0
3d	236.9	432.5	677.8	972.5	1 506.3
4p	105.5	206.5	335.7	492.9	780.2

electrons, $U_{\rm el}(r)$, is calculated using the Hartree–Fock wavefunctions. For $\varepsilon_1 = 0.01$–5 keV the effective charge $Z_{\rm eff}$ varies between 8 and 22 in the case of Kr^{8+}, and between 27 and 35 for Xe^{26+}. It is obvious that the values obtained from equation (2), and shown in figures 6(c) and (d), overestimate the true ratio of the cross sections (figures 6(a) and (b)) by orders of magnitude.

This discrepancy can also be seen if we use a simple estimate for $[\omega^2\alpha(\omega)/Z_{\rm eff}]^2$. For photon energies between the $n = 2$ and $n = 3$ thresholds, the quantity $-\omega^2\alpha(\omega)$ is approximately equal to 18, i.e. the number of electrons in the 3s, 3p and 3d subshells, while for $I_{2s,2p} \ll \omega \ll I_{1s}$, it is approximately 26 (the number of electrons in all subshells but 1s). Here $I_{1s}, I_{2s}, \ldots$ are the ionization potentials of the subshells (see table 1). Hence, one can write the following estimate $[\omega^2\alpha(\omega)/Z_{\rm eff}]^2 \approx (N/Z_{\rm eff})^2$. The values of $(N/Z_{\rm eff})^2$ are shown

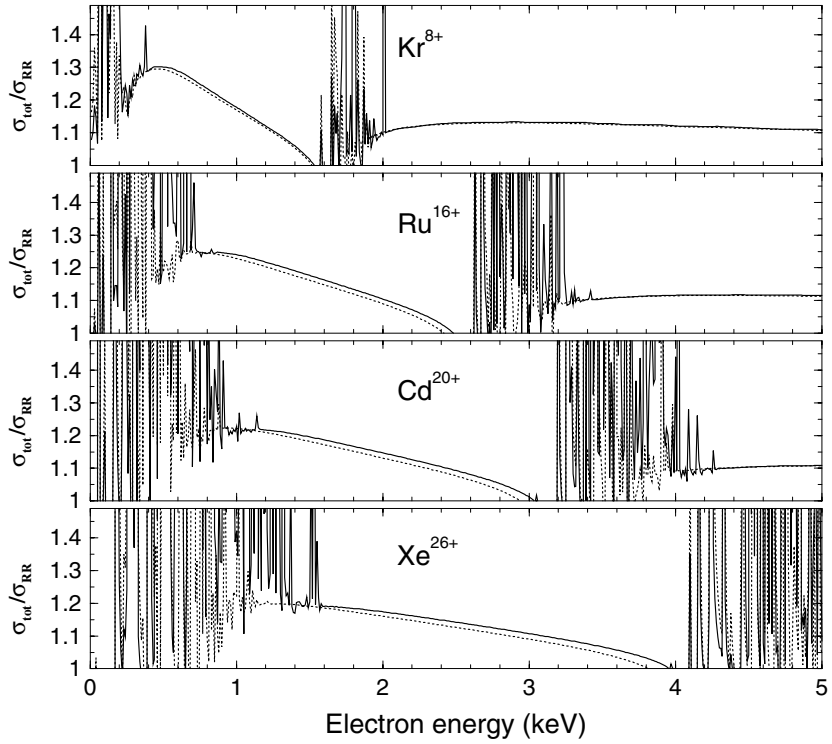

Figure 7. Ratios $\sigma_{\rm tot}/\sigma_{\rm RR}$ for the Ni-like ions. Dotted curves correspond to $\sigma_{\rm tot}(4)/\sigma_{\rm RR}(4)$, while solid curves show $\sigma_{\rm tot}(4\text{–}10)/\sigma_{\rm RR}(4\text{–}10)$.

in figures 6(c) and (d) by dashed lines. They are comparable to the values of $[\omega^2\alpha(\omega)/Z_{\rm eff}]^2$ calculated accurately, which confirms that equation (2) cannot be relied upon to estimate the PR cross section.

In order to appreciate the true role of PR, the ratios $\sigma_{\rm tot}(4)/\sigma_{\rm RR}(4)$ and $\sigma_{\rm tot}(4\text{–}10)/\sigma_{\rm RR}(4\text{–}10)$ are plotted in figure 7 as functions of the electron energy. As observed above, PR leads to enhanced recombination cross sections in the non-resonant regions, mainly due to the interference term $\sigma_{\rm int}$ (see equation (21)). The interference nature of the PR effect can also be inferred from the dip which occurs at energies just below the region of $n = 2$ dielectronic excitations. Here the PR effect leads to a destructive interference.

The actual value of the enhancement due to PR is about 10 to 30%. It depends on the energy but changes little along the isoelectronic sequence. A comparison between the selective and total recombination cross sections (shown in figure 7 by dotted and solid curves, respectively), and, also, between $\sigma_{\rm tot}$ and $\sigma_{\rm RR}$ calculated for different n_2 (figure 5) shows that the ratio $\sigma_{\rm tot}/\sigma_{\rm RR}$ depends weakly on the principal quantum number of the final electron state. This indicates that the main contribution to the radial integrals $r_{\nu_2\nu_1}$ and $V^{(1)}_{n2,10}$, equations (11*b*), (11*a*) and (12), which determine the RR and PR partial amplitudes, comes from small distances r (much smaller than the mean radius of the final-state orbitals with $n_2 = 4$).

3.2. 'Stripping' approximation

To understand the enhancement of $\sigma_{\rm tot}$ over $\sigma_{\rm RR}$ in non-resonant energy regions qualitatively, one can use arguments similar to those developed in the theory of polarizational bremsstrahlung, where the analogous effect (Buimistrov and Trakhtenberg 1977, Amusia

et al 1985, Korol 1992, Korol *et al* 2002) is known as the 'stripping' phenomenon (Amusia *et al* 1985).

For a fixed energy ε_2 of the captured electron, the initial energy ε_1 defines that of the emitted photon, $\omega = \varepsilon_1 - \varepsilon_2$. In a many-electron target where the ionization potentials of different subshells are well separated, the electrons can be divided into two groups, the 'inner' and the 'outer' electrons, with respect to ω. The inner electrons are those whose binding energies, $I_{\rm in}$, exceed ω. Conversely, the outer electrons have binding energies $I_{\rm out}$ less than ω:

$$I_{\rm out} < \omega < I_{\rm in}. \tag{22}$$

The cloud of strongly bound inner electrons is weakly distorted, or polarized, by an external electromagnetic field of frequency ω. Therefore, assuming the strong inequality $\omega \ll I_{\rm in}$, one can neglect the contribution of the virtual excitations of the inner electrons to the sum in (6). Then, the amplitude $F_{\rm PR}$ can be approximated by the contribution of the outer-shell electrons alone

$$F_{\rm PR} \approx -\sum_{a,a'=1}^{N_{\rm out}} \sum_{n} \left[\frac{\langle 0|\mathbf{e}\cdot\mathbf{r}_a|n\rangle\langle n;\,2|v_{a'}|1;\,0\rangle}{\omega_{n0}-\omega} + \frac{\langle 0;\,2|v_{a'}|1;\,n\rangle\langle n|\mathbf{e}\cdot\mathbf{r}_a|0\rangle}{\omega_{n0}+\omega} \right], \tag{23}$$

where $N_{\rm out}$ is the number of such electrons.

Assuming the strong inequality $\omega \gg I_{\rm out}$ as well, one can expand the denominators in powers of the small parameter $\omega_{n0}/\omega \sim I_{\rm out}/\omega$. The leading term, proportional to ω^{-2}, is evaluated with the help of closure $\sum_n |n\rangle\langle n| = 1$. The result is

$$F_{\rm PR} \approx \frac{1}{\omega^2}\langle 2|\mathbf{e}\cdot\mathbf{a}_{\rm out}|1\rangle, \tag{24}$$

where $\mathbf{a}_{\rm out}$ is the acceleration due to the static field of the outer electrons (Korol *et al* 2002).

To obtain the final expression for $F_{\rm tot}$, let us introduce the operator of the total acceleration $\mathbf{a}$ of the electron in the field of the ion:

$$\mathbf{a} = -Z\frac{\mathbf{r}}{r^3} + \mathbf{a}_{\rm in} + \mathbf{a}_{\rm out}, \tag{25}$$

where $\mathbf{a}_{\rm in}$ is the acceleration due to the potential created by the inner electrons. With the help of the relation between the dipole matrix elements in the 'length' and 'acceleration' forms (see, e.g., Sobelman (1992)), the RR amplitude (5) can be cast in the form

$$F_{\rm RR} = -\frac{1}{\omega^2}\langle 2|\mathbf{e}\cdot\mathbf{a}|1\rangle. \tag{26}$$

Taking into account equation (24), one obtains the following approximate formula for the total amplitude:

$$F_{\rm tot} \approx -\frac{1}{\omega^2}\langle 2|\mathbf{e}\cdot\mathbf{a}_{\rm eff}|1\rangle, \tag{27}$$

where

$$\mathbf{a}_{\rm eff} = -Z\frac{\mathbf{r}}{r^3} + \mathbf{a}_{\rm in} \tag{28}$$

is the effective acceleration.

Comparing (26) with (27) one notes that the latter does not contain the acceleration due to the outer electrons. Hence, in $F_{\rm tot}$ the outer electrons do not participate in the screening of the nucleus (or, in other words, the ion is 'stripped' of its $N_{\rm out}$ outer electrons). As a result, the cross section of the radiative capture is *enhanced* compared with $\sigma_{\rm RR}$, since the effective acceleration of the projectile becomes larger. A physical origin of 'stripping' is in that for $\omega \gg I_{\rm out}$ the outer electrons can be considered as quasi-free, which means that there is no

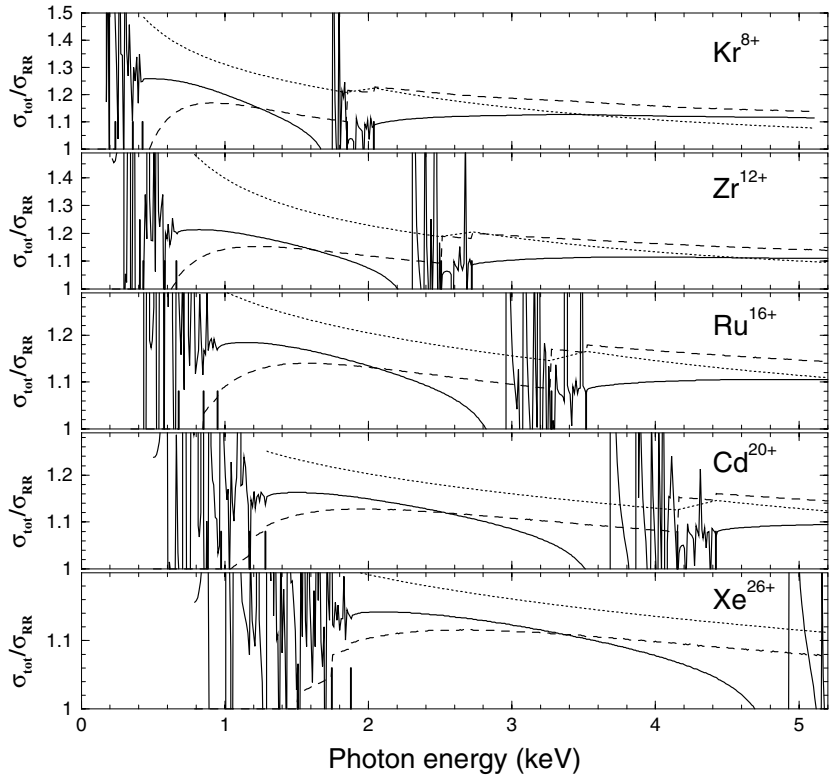

Figure 8. Ratio $\sigma_{\rm tot}/\sigma_{\rm RR}$ for the selective capture into the 4p states of Ni-like ions as a function of the photon energy ω. The ratios shown by solid curves were obtained using the exact form of the total amplitude, equations (6) and (7). Dashed curves correspond to the stripping approximation (27), while dotted curves show the results obtained from equation (32). Vertical bars (in some cases obscured by the resonances) indicate the Hartree–Fock ionization energies of the orbitals.

dipole photon emission from the system 'incident electron plus outer electrons' (see, e.g., Landau and Lifshitz (1971)). In other words, the radiation of the incident and outer electrons, due to their interaction with each other, cancels out.

It is interesting to test the effect of 'stripping' quantitatively. In figure 8 we show the ratios $\sigma_{\rm tot}({\rm 4p})/\sigma_{\rm RR}({\rm 4p})$ calculated using different approximations, as functions of the photon energy $\omega = \varepsilon_1 - I_{\rm 4p}$, for the Ni-like ions. Solid curves indicate the value obtained by using the exact amplitude $F_{\rm PR}$, equations (5), (6) and (8), while the dashed curves correspond to the 'stripping' approximation for the total amplitude, equation (27). In implementing this equation, we drop the contributions of the outer subshells successively, as the photon energy crosses their ionization thresholds.

We see that the 'stripping' approximation provides a correct estimate of the PR effect away from the thresholds, in the energy intervals $I_{\rm 3d,3p,3s} < \omega < I_{\rm 2p,2s}$ and $\omega > I_{\rm 2p,2s}$. Close to the thresholds the polarizational amplitude has a strong energy dependence, because of the resonant denominators, see equation (6). This feature is obviously not accounted for by the 'stripping' approximation.

Thus, the role of the target polarization can be described in terms of 'stripping'. However, it would be useful to have an even simpler way of estimating the role of polarization. Below we derive an analytical estimate for the ratio $\sigma_{\rm tot}/\sigma_{\rm RR}$, based on the 'stripping' approximation and on the use of the arguments of the so-called Kramers electrodynamics (Kogan *et al* 1992).

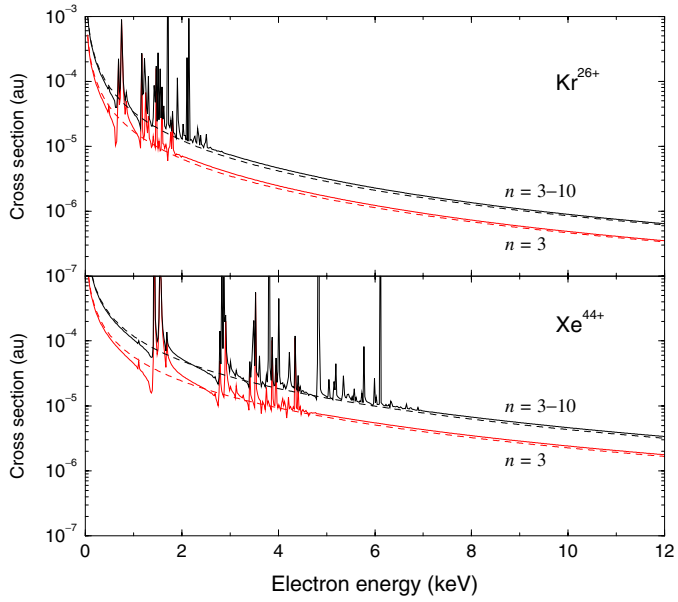

Figure 9. Recombination cross sections $\sigma_{\rm tot}$ (solid curves) and $\sigma_{\rm RR}$ (dashed curves) for Ne-like Kr^{26+} and Xe^{44+}. Red curves represent the cross sections $\sigma(3) = \sum_{l=0}^{3} \sigma(3l)$, while black curves are the cross sections summed over all n from 3 to 10, and over the corresponding l-values.

Let us first re-write equation (24) as

$$F_{\rm PR} \approx \frac{1}{\omega^2} \left\langle 2 \left| \mathbf{e}\cdot\mathbf{r} \frac{N_{\rm out}(r)}{r^3} \right| 1 \right\rangle, \tag{29}$$

where $N_{\rm out}(r) = 4\pi \int_0^r \rho_{\rm out}(r') r'^2 \, {\rm d}r'$ is the number of outer-shell electrons within the sphere of radius r, and $\rho_{\rm out}$ is their density.

To estimate the size of $F_{\rm PR}$ relative to $F_{\rm RR} = \langle 2|\mathbf{e}\cdot\mathbf{r}|1\rangle$, we want to extract the factor $N_{\rm out}(r)/r^3$, taken at some point $r = r_0$, from the matrix element (29). The choice of r_0 is determined by the condition that the distances $r \sim r_0$ contribute most effectively to the matrix element.

The matrix element in equation (29) describes a radiative transition from the continuum state '1' into the bound state '2' under the action of an effective operator. According to the quasi-classical theory of radiative transitions (Kogan *et al* 1992), the emission of electromagnetic waves of frequency ω by a charged particle is most effective in the vicinity of the turning points of classical trajectories for which the particle's angular velocity at these points is close to ω. Therefore, the distance r_0 can be estimated as a root of equation (3). The right-hand side of equation (29) then becomes

$$F_{\rm PR} \approx \langle 2|\mathbf{e}\cdot\mathbf{r}|1\rangle \frac{N_{\rm out}(r_0)}{\omega^2 r_0^3} = F_{\rm RR} \frac{N_{\rm out}(r_0)}{\omega^2 r_0^3}, \tag{30}$$

and the total amplitude is written as

$$F_{\rm tot} \approx F_{\rm RR} \left(1 + \frac{N_{\rm out}(r_0)}{\omega^2 r_0^3} \right). \tag{31}$$

This gives the following estimate:

$$\frac{\sigma_{\rm tot}}{\sigma_{\rm RR}} \approx 1 + \frac{2N_{\rm out}(r_0)}{\omega^2 r_0^3}, \tag{32}$$

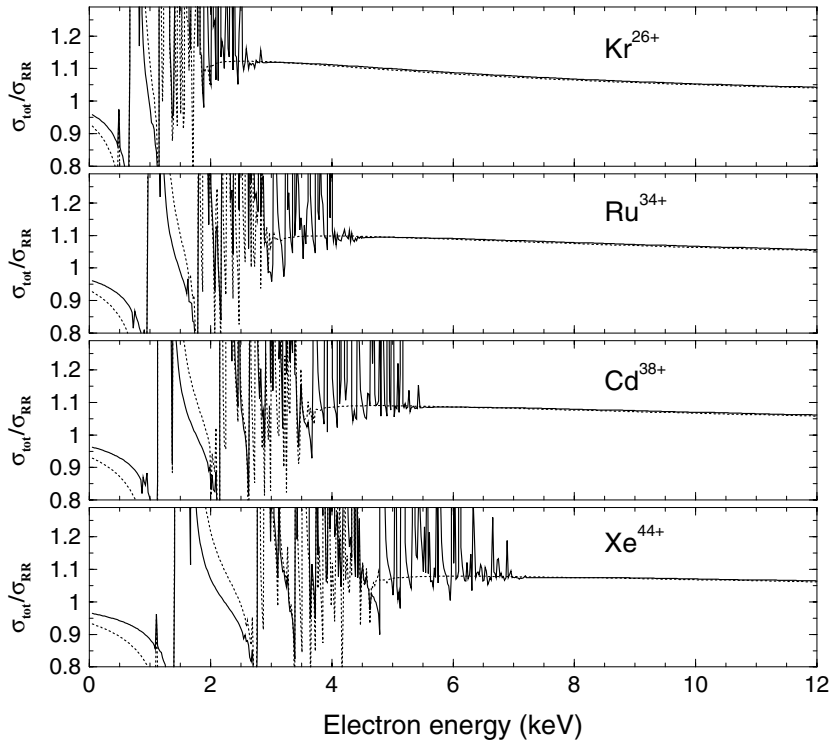

Figure 10. Dependence of the ratios $\sigma_{\rm tot}/\sigma_{\rm RR}$ on the electron energy for Ne-like ions. Dotted curves depict $\sigma_{\rm tot}(3)/\sigma_{\rm RR}(3)$, while solid curves correspond to the ratios of cross sections summed over the final states, $\sigma_{\rm tot}(3\text{–}10)/\sigma_{\rm RR}(3\text{–}10)$.

where we have assumed that the second term in brackets in equation (31) is a small correction. The second term on the right-hand side of equation (32) corresponds to the ratio $\sigma_{\rm int}/\sigma_{\rm RR}$, cf equation (21).

The results obtained from equation (32) are shown in figure 8 by dotted curves. Comparing these to the accurate numerical results (solid curves) one concludes that in spite of its simplicity, equation (32) yields a reasonable estimate for the ratio $\sigma_{\rm tot}/\sigma_{\rm RR}$ in the non-resonant regions.

3.3. Ne-like ions

Numerical calculations of the recombination cross sections have also been performed for a number of Ne-like ions: Kr^{26+}, Zr^{30+}, Ru^{34+}, Sr^{38+}, Xe^{44+} and Ba^{46+}. They show that, as in the case of Ni-like targets, the PR mechanism leads to an increase of the cross section in the non-resonant regions, see figure 9. As before, this increase is due to constructive interference between the RR and PR amplitudes. However, for a Ne-like target with a given Z, the ratio $\sigma_{\rm tot}/\sigma_{\rm RR}$ is smaller than that for the corresponding Ni-like ion. The decrease of the relative role of polarization and the interference term $\sigma_{\rm int}$ with the ionicity Z_0 could be expected. We can deduce an explicit dependence of the ratio $\sigma_{\rm int}/\sigma_{\rm RR}$ on Z_0 from (32). Let us first approximate the factor $N_{\rm out}(r_0)/r_0^3$ by $N_{\rm out}/R_{\rm out}^3$, $R_{\rm out}$ being the (average) radius of the outer electrons. Using $R_{\rm out} \sim Z_0/I_{\rm out}$ and $I_{\rm out} \sim Z_0^2$, we derive $\sigma_{\rm int}/\sigma_{\rm RR} \sim (N_{\rm out}/Z_0)\big(I_{\rm out}^2/\omega^2\big)$. Hence, for a fixed number of outer electrons and for a given $I_{\rm out}/\omega$ ratio, the relative magnitude of $\sigma_{\rm int}$ decreases as Z_0^{-1}. This conclusion is confirmed by the result presented in figures 9 and 10.

In figure 9 the cross sections $\sigma_{\rm tot}(3)$, $\sigma_{\rm RR}(3)$ and $\sigma_{\rm tot}(3\text{–}10)$, $\sigma_{\rm RR}(3\text{–}10)$ are plotted for Kr^{26+} and Xe^{44+} ions. Sharp peaks in $\sigma_{\rm tot}$ correspond to discrete ionic excitations from the 2s and 2p shells. We observe that $\sigma_{\rm tot}$ is greater than $\sigma_{\rm RR}$ outside the resonance regions, although this enhancement is less pronounced than in the case of Ni-like Kr and Xe ions (figures 3–5).

The ratios $\sigma_{\rm tot}(3)/\sigma_{\rm RR}(3)$ and $\sigma_{\rm tot}(3\text{–}10)/\sigma_{\rm RR}(3\text{–}10)$ versus the electron energy are plotted in figure 10. As for the Ni-like targets (figure 7), the recombination cross section is enhanced in the non-resonant regions due to the polarizational mechanism. The actual size of this enhancement varies between 5 and 15%. Similar to the Ni-like case, the ratio $\sigma_{\rm tot}/\sigma_{\rm RR}$ depends weakly on the principal quantum number of the final electron state. It is also worth noting that the polarization contribution results in a prominent dip in $\sigma_{\rm tot}$ at the energy just below the dielectronic resonance region.

4. Conclusions

We have demonstrated that for electron energies outside the regions of DR resonances, the cross sections of electron–ion recombination are enhanced due to the constructive interference of the photons emitted via the radiative recombination and the polarizational recombination mechanisms. For multiply charged targets this enhancement, which is characterized by the ratio $\sigma_{\rm int}/\sigma_{\rm RR}$, varies from a few per cent to a few tens of per cent, depending on the ionicity and on the energy of the incident electron. The values for $\sigma_{\rm int}/\sigma_{\rm RR}$ obtained in this paper indicate that the contribution of the polarizational recombination channel is sufficiently large and could be detected experimentally. The enhancement due to PR needs to be taken into account in order to obtain accurate absolute values of the recombination cross sections between the DR resonance regions. However, the size of the enhancement is orders of magnitudes smaller than predicted by Bureeva and Lisitsa (1998, 1999) and Astapenko *et al* (2000, 2002).

In the present paper we restricted ourselves to the cases of Ni- and Ne-like ions. In the former case the ionic core is less rigid and is polarized more efficiently. It would be interesting to carry out a wider survey of the effect of polarization recombination, by analysing ionic targets of other isoelectronic sequences, over wider ranges of electron energies and at lower ionicities, where the role of target polarization is stronger.

Acknowledgments

The work of AK has been supported by the Distinguished Visiting Fellowship programme at the International Research Centre for Experimental Physics (Queen's University Belfast), and the authors are grateful for this support. We also thank Dr Brian O'Rourke for useful discussions.

References

Amusia M Ya 1982 *Comm. At. Phys.* **11** 123
Amusia M Ya 1988 *Phys. Rep.* **142** 269–335
Amusia M Ya, Avdonina N B, Chernysheva L V and Kuchiev M Yu 1985 *J. Phys. B: At. Mol. Phys.* **18** L791–6
Astapenko V A, Bureeva L and Lisitsa V 2000 *Phys. Scr.* T **86** 62–7
Astapenko V A, Bureeva L and Lisitsa V 2002 *Usp. Fiz. Nauk* **172** 155–92
Berestetsky V B, Lifshitz E M and Pitaevsky L P 1982 *Quantum Electrodynamics* (Oxford: Pergamon)
Buimistrov V M and Trakhtenberg L I 1977 *Zh. Eksp. Teor. Fiz.* **23** 850–3
Buimistrov V M and Trakhtenberg L I 1977 *Sov. Phys.—JETP* **46** 447–8 (Engl. Transl.)
Bureeva L and Lisitsa V 1998 *J. Phys. B: At. Mol. Opt. Phys.* **31** 1477–85
Bureeva L and Lisitsa V 1999 *Phys. Scr.* T **80** 163–4

Connerade J P and Solov'yov A V 1996 *J. Phys. B: At. Mol. Opt. Phys.* **29** 365–75
DeWitt D R *et al* 1994 *Phys. Rev.* A **50** 1257
Gribakin G F and Korol A V 2001 *XXII Int. Conf. on the Physics of Electronic and Atomic Collisions (Santa Fe, NM, July 2001)* Book of Abstracts p 341
Hahn Y 1997 *Rep. Prog. Phys.* **60** 691–759
Hoffknecht A *et al* 1998 *J. Phys. B: At. Mol. Opt. Phys.* **31** 2415
Kilgus G *et al* 1992 *Phys. Rev.* A **46** 5730
Kogan V I, Kukushkin A B and Lisitsa V S 1992 *Phys. Rep.* **213** 1
Korol A V 1992 *J. Phys. B: At. Mol. Opt. Phys.* **25** L341–4
Korol A V, Lyalin A G and Solov'yov A V 1997 *J. Phys. B: At. Mol. Opt. Phys.* **30** L115–21
Korol A V, Lyalin A G, Solovyov A V, Avdonina N B and Pratt R H 2002 *J. Phys. B: At. Mol. Opt. Phys.* **35** 1197–210
Korol A V and Solov'yov A V 1997 *J. Phys. B: At. Mol. Opt. Phys.* **30** 1105–50
Landau L D and Lifshitz E M 1971 *The Classical Theory of Fields* (Oxford: Pergamon)
Landau L D and Lifshitz E M 1977 *Quantum Mechanics* (Oxford: Pergamon)
O'Rourke B E, Kuramoto H, Li Y M, Ohtani S, Tong X M, Watanabe H and Currell F J 2004 *J. Phys. B: At. Mol. Opt. Phys.* **37** 2343
Schenach S *et al* 1994 *Z. Phys.* D **30** 291
Schippers S *et al* 2002 *Phys. Rev.* A **65** 042723
Schnell M *et al* 2003 *Phys. Rev. Lett.* **91** 043001
Schuch R, Fogle M, Glans P, Lindroth E, Madzunkov S, Mohamed T and Nikolic D 2003 *Radiat. Phys. Chem.* **68** 51
Sobelman I I 1992 *Atomic Spectra and Radiative Transitions* (Berlin: Springer)
Smith A J, Beiersdorfer P, Widmann K, Chen M H and Scofield J H 2000 *Phys. Rev.* A **62** 052717
Tokman M *et al* 2002 *Phys. Rev.* A **66** 012703
Varshalovich D A, Moskalev A N and Khersonskii V K 1988 *Quantum Theory of Angular Momentum* (Singapore: World Scientific)
Watanabe H, Currell F J, Kuramoto H, Ohtani S, O'Rourke B E and Tong X M 2002 *J. Phys. B: At. Mol. Opt. Phys.* **35** 5095
Zon B A 1977 *Sov. Phys.—JETP* **46** 65